

# Inverse Kinetic Effects: localization and re-entrant transitions

Roopayan Ghosh,<sup>1,\*</sup> Madhumita Sarkar,<sup>2</sup> and Ivan M. Khaymovich<sup>3,4</sup>

<sup>1</sup>*Department of Physics and Astronomy, University College London, Gower Street, WC1E6BT, London*

<sup>2</sup>*Department of Physics and Astronomy, University of Exeter,  
Stocker Road, Exeter EX4 4QL, United Kingdom*

<sup>3</sup>*Nordita, Stockholm University and KTH Royal Institute of Technology Hannes Alfvéns väg 12, SE-106 91 Stockholm, Sweden*

<sup>4</sup>*Institute for Physics of Microstructures, Russian Academy of Sciences, 603950 Nizhny Novgorod, GSP-105, Russia*

Typically, metallic systems localized under strong disorder exhibit a transition to finite conduction as kinetic terms increase. In this work, we reveal the opposite effect – increasing kinetic terms leads to an unexpected suppression of conductivity, enhancing localization of the system, and even lead to re-entrant delocalization transitions. Specifically, we add a nearest-neighbor hopping with amplitude  $\kappa$  to the Rosenzweig-Porter (RP) model with fractal on-site disorder and surprisingly see that, as  $\kappa$  grows, the system initially tends to localization from the fractal phase, but then re-enters the ergodic phase. We build an analytical framework to explain this re-entrant behavior, supported by exact diagonalization results. The interplay between the spatially local  $\kappa$  term, insensitive to fractal disorder, and the energy-local RP coupling, sensitive to fine-level spacing structure, drives the observed re-entrant behavior. This mechanism offers a novel pathway to re-entrant localization phenomena in many-body quantum systems.

**Introduction:** Ergodicity in quantum many-body systems [1, 2] and its breakdown by the disordered potential [3–5], usually called the many-body localization (MBL) transition has attracted a lot of attention for the past two decades. This stems both from fundamental challenges in determining whether the MBL phase persists in the thermodynamic limit [6–12], and from the potential applications of this phase in quantum information processing and machine learning [13, 14].

According to common knowledge, disordered quantum systems typically exhibit localization behavior, such as in Anderson transition [15] and many-body localization [3, 4], which occur monotonically with increasing the disorder strength (or equivalently, decreasing the amplitude of the corresponding kinetic term). This behavior is believed to be universal both in many-body disordered systems [5] and in the corresponding random-matrix (RM) ensembles utilized to understand them with Anderson [16] and ergodicity breaking [17] phase transitions. The latter models, like the so-called Rosenzweig-Porter random-matrix ensemble [17–24], show not only Anderson localized and ergodic (metallic) phases, but also an intermediate non-ergodic extended phase (relevant for the description of the Hilbert-space structure of the MBL states [25–27]), in which the eigenstates span over an extensive number but measure zero of all Hilbert-space configurations characterized by fractal dimensions  $0 \leq D_2 \leq 1$ , see Eq. (2) [16]. In this letter, using RM ensembles, we analytically reveal a pathway that challenges the conventional view of a monotonic transition from localization to ergodicity. Starting with a system characterized by a fractal distribution of on-site disorder [28, 29], we show that adding a short-range kinetic term with coupling strength  $\kappa$  initially steers the system towards localization. Only beyond a critical strength of  $\kappa$ , this trend reverses, and further increasing  $\kappa$  drives the

system to an ergodic phase, see Fig. 1. Our analytical understanding provides a new perspective on re-entrant delocalization transitions, a phenomenon not previously explored in the literature. We then verify our predictions with exact numerical simulations.

**Model:** The standard Rosenzweig-Porter model [17, 30] is a random-matrix model where both the diagonal and off-diagonal elements of the  $L \times L$  Hermitian matrix  $H_{mn} = H_{nm}^*$  are taken from a random normal distribution such that,

$$H_{mn} = h_n \delta_{mn} + R_{mn} \cdot L^{-\gamma/2}. \quad (1)$$

Here  $\overline{h_n} = \overline{R_{mn}} = 0$  and  $\overline{h_n^2} = \overline{R_{mn}^2} = 1$  and  $\gamma$  is the tuning parameter which rescales the off-diagonal elements and controls the phase diagram. The ergodic ( $\gamma \leq 1$ ) and localized ( $\gamma \geq 2$ ) phases are separated by a non-ergodic extended fractal phase ( $1 \leq \gamma \leq 2$ ), which is squeezed between the ergodic transition (ET) at  $\gamma = 1$  and the Anderson localization transition (AT) at  $\gamma = 2$ . The eigenstate nature in different phases can be characterized by the fractal dimension  $D_2$ , calculated from the eigenfunctions  $|\psi\rangle$ , as [16]

$$L^{-D_2} = \text{IPR} = \sum_{i=1}^L |\langle i|\psi\rangle|^4 \quad (2)$$

where  $|i\rangle$  denotes the computational basis states and IPR denotes the inverse participation ratio. The ergodic states are characterized by  $D_2 = 1$ , the extended (multi)fractal states are characterized by  $0 < D_2 < 1$  and for the localized state  $D_2 = 0$ . Recently it has been shown [29] that the fractal distribution of diagonal elements  $h_n$ 's tunes the phase diagram of the Rosenzweig-Porter (RP) model by extending the non-ergodic fractal phase. Simply put, in this scenario one considers  $s_n = h_{n+1} - h_n$  distributed as a Pareto distribution

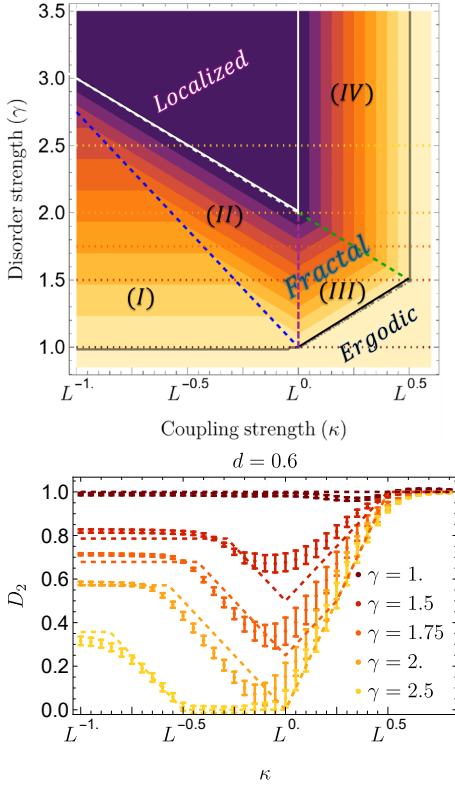


FIG. 1. (a) Localization phase diagram in terms of fractal dimension  $D_2$  for  $d = 0.6$  for different nearest neighbor coupling  $\kappa$  and effective disorder strength ( $\gamma$ ), obtained from exact analytical computation. The localized and fractal phases are separated by the white line and the fractal and ergodic phases are separated by the black line. Inside the fractal phase the regions with different behavior are separated by dashed lines and marked with roman numerals. The horizontal dotted lines denote the values of  $\gamma$  chosen for (b). (b)  $D_2$  with varying  $\kappa$  for specific  $\gamma$ s. The numerical data shown via points are obtained by fitting IPR for different system sizes  $2^n$  where  $n$  runs from 7–14 and averaged over  $10^2$ – $10^5$  realizations (the smaller system sizes have larger number of realizations). The dashed lines denote the analytical results.

$P(s) = \frac{d \cdot \delta_{typ}^d}{s^{d+1}} \theta(s - \delta_{typ})$  where  $\delta_{typ} \sim L^{-1/d}$  is the typical level spacing. Consequently, the number of elements  $h_n$  in the interval  $L^{-b}$  around a certain energy  $E$  scales as  $N\{|E - h_n| \in [L^{-b-db}, L^{-b}]\} \sim L^{1-f(b)db}$ , where  $f(x) = d \cdot x$ ,  $df(x)/dx \leq 1$  for Hermitian matrices,  $f(0) = 0$  and  $d$  can be regarded as the fractal dimension of the disorder. In this work, we add an extra nearest-neighbor hopping term to modify Eq. (1) to:

$$H_{mn} = h_n \delta_{mn} + \kappa (\delta_{m,n+1} + h.c.) + R_{mn} L^{-\gamma/2}, \quad (3)$$

where  $h_n$  is distributed as fractal disorder (see Appendix A), and the amplitude of the extra nearest-neighbor hopping term scales with the system size,  $\kappa \sim L^k$ , with positive or negative  $k$ . We shall discuss the

non-monotonic fractal dimension behavior by tuning this extra term  $k$  in what follows.

**Phase diagram:** By increasing the nearest-neighbor hopping strength  $\kappa$  from zero, a strikingly counterintuitive phenomenon occurs. For small but significant coupling, the fractal dimension  $D_2$  initially decreases, driving the system towards localization. Only beyond a certain critical hopping amplitude  $\kappa$  does the standard increasing behavior of  $D_2$  (indicating more delocalization) dominates. This reveals a rich re-entrant phase diagram as shown in Fig. 1(a), where we plot the fractal dimension ( $D_2$ ) vs varying coupling strength ( $\kappa$ ) and disorder strength (which is controlled by  $\gamma$ ), see [31] for results for other values of  $d$ . From a fully analytic study described later, we compute the fractal dimension  $D_2$  of the different regions of the diagram as follows:

**Region 1:** For  $k > 0$ ,  $\kappa \gg 1$  there are no effects of the fractal diagonal disorder:

$$D_2(\gamma) = \begin{cases} 1, & \gamma < \gamma_{ET}^{(1)}, \\ 2 - \gamma + k, & \gamma_{ET}^{(1)} < \gamma < \gamma_P, \\ 2k, & \gamma_P < \gamma. \end{cases}, \quad (4)$$

because of the spatial locality of the dominant hopping term  $\kappa$ . Here, there is no localized phase, only the ergodic,  $\gamma < \gamma_{ET}^{(1)} = 1 + k$ , and fractal phases. We distinguish the two fractal phases as RP-like (**fractal III** in Fig. 1(a)) for the middle regime, and block-like (**fractal IV**),  $\gamma > \gamma_P = 2 - k$ , for the final regime in Fig. 1(a). This is because fractal IV has energy level spacings distributed according to Poisson statistics in spite of it not being localized, distinct from the other regime. The middle regime disappears at  $k = 1/2$  and the system becomes ergodic for all  $k > 1/2$  at any  $\gamma$ .

**Region 2:** For intermediate  $-(1+d)/(2d) < k < 0$ , there is competition between the hopping terms and the fractal disorder resulting in four distinct regimes of  $\gamma$ :

$$D_2(\gamma) = \begin{cases} 1, & \gamma < \gamma_{ET}^{(2)}, \\ \frac{2-d\gamma}{2-d}, & \gamma_{ET}^{(2)} < \gamma < \gamma_{FT}, \\ 2 - \gamma + |2k| \frac{2-2d}{1+d}, & \gamma_{FT} < \gamma < \gamma_{AT}^{(2)}, \\ 0, & \gamma_{AT}^{(2)} < \gamma \end{cases}, \quad (5)$$

ergodic,  $\gamma < \gamma_{ET}^{(2)} = 1$  and localized,  $\gamma > \gamma_{AT}^{(2)} = 2 + \frac{2-2d}{1+d} |2k|$  ones are complimented by two fractal phases: the fractal-disorder-dominated [29],  $\gamma < \gamma_{FT} = 1 + \frac{2-d}{1+d} |2k|$  (**fractal I** in Fig. 1(a)) and the standard RP-like [17],  $\gamma > \gamma_{FT}$  denoted by **fractal II** in Fig. 1(a) to distinguish their origins.

**Region 3:** For small  $k < -(1+d)/(2d)$ , there are no effects of the short-range hopping and the results coincide with the ones of [29] with the enlarged fractal-disorder-dominated phase, also denoted by **fractal I**:

$$D_2(\gamma) = \begin{cases} 1, & \gamma < \gamma_{ET}^{(3)}, \\ \frac{2-d\gamma}{2-d}, & \gamma_{ET}^{(3)} < \gamma < \gamma_{AT}^{(3)}, \\ 0, & \gamma_{AT}^{(3)} < \gamma. \end{cases}, \quad (6)$$

with  $\gamma_{ET}^{(3)} = 1$  and  $\gamma_{AT}^{(3)} = 2/d$ .

The re-entrant behavior is even more evident in Fig. 1(b) by considering fixed  $\gamma$  cuts from Fig. 1(a), marked by the red dotted lines on the plot. The numerical data, represented by points, aligns well with the analytical prediction of the phase diagram outlined above, which is plotted alongside the data with dashed lines. As is clearly evident for  $\gamma > 1$   $D_2$  shows a reduction with increasing value of  $\kappa$  first, before reverting back to the standard behavior towards delocalization.

In what follows, we provide a detailed analytical explanation for the different regions of the phase diagram. In summary, the key insight lies in identifying how the nearest-neighbor coupling hybridizes the fractal RP eigenstates, thereby modifying the spectral distribution. In certain parameter regimes, due to the hybridization, the effective on-site disorder distribution is transformed from correlated fractal to uncorrelated Gaussian, which triggers localization. We shall treat the cases  $k > 0$  and  $k < 0$  separately, as they give rise to distinct phenomena.

**Analytical explanation:** Let us first recall the main results for  $\kappa = 0$  i.e.  $k \rightarrow -\infty$ , the fractal RP model limit. The eigenfunction of any RP model has a Lorentzian structure [20, 21, 32] (including the fractal disorder case [29])

$$|\psi_m(n)|^2 = \frac{A}{(h_n - E_m)^2 + \Gamma_d^2} \quad (7)$$

where  $A$  is the normalization coefficient. We also have  $\Gamma_d \sim L^{-a}$  with the parameter  $a$  being the solution of the self-consistency equation

$$1 + 2a - f(a) = \gamma. \quad (8)$$

Clearly,  $\Gamma_d$  is the width of the eigenfunction miniband, within which all the eigenstates are fully hybridized, and is found to be [29].

$$\Gamma_d \sim L^{-\frac{\gamma-1}{2-d}} \quad (9)$$

For small enough short-range hopping  $\kappa$ , the fractal phase is dominated by the local-in-energy RP broadening  $\Gamma_d$  [17], highly sensitive to the fractal on-site disorder [29]. At large  $\kappa \gtrsim 1$ , the standard picture of 1D Anderson prevails [33], removing all the fine (fractal) details of the diagonal-energy distribution via strong short-range resonances. In the intermediate region the competition between  $\Gamma_d$  and  $\kappa$  comes into play and gradually destroys the fractal structure of the diagonal disorder: the interplay between two delocalizing mechanisms reduces the fractal dimension and can even localize the system. Let us now consider the situation in details for the two different limits,

**Region 1 ( $k > 0 \implies \kappa \gg 1$ ):** When  $\kappa \gg 1$ , the nearest-neighbor term dominates the Hamiltonian and strongly hybridizes nearby sites, effectively creating a

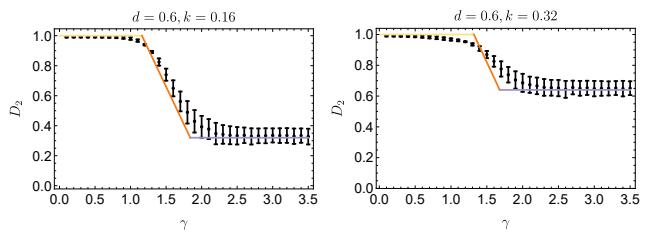


FIG. 2. Comparison of numerically computed variation fractal dimension  $D_2$  with  $\gamma$  (points with error bars) to analytically computed Eq. (4) (solid lines) for  $k = 0.16$  and  $k = 0.32$ . the orange (lilac) line denotes fractal III (IV) phase, yellow line stands for the ergodic phase.

block diagonal structure in the Hamiltonian, before the effects of RP-coupling kick in. The block sizes scale as  $\xi \sim \kappa^2 = L^{2k} \gg 1$ , see [33, 34], where  $\xi$  is the localization length in an effective 1D Anderson model with disorder strength  $\kappa^{-1}$  [33, 35]. Within each block, wave functions become fully hybridized, rendering the fractal disorder distribution in diagonal elements  $h_n$  insignificant. The bandwidth of the  $\xi \times \xi$  block is equal to the total bandwidth and can be estimated as,  $E_{BW}^2 = \frac{1}{L} \sum_{m,n=1}^L \langle |H_{mn}|^2 \rangle = \frac{1}{\xi} \sum_{m,n=1}^{\xi} \langle |H_{mn}|^2 \rangle = 2\kappa^2 + 1$ . The corresponding mean level spacing  $\delta_\xi$  in each of such blocks reads as  $\delta_\xi \simeq \frac{E_{BW}}{\xi}$ , as the number of levels in each block is given by the block size  $\xi$ .

Using  $\kappa \sim \xi^{1/2} \gg 1$ , we have  $E_{BW} \simeq \xi^{1/2}$ . Therefore the local level spacing in each block,  $\delta_\xi \sim \xi^{-1/2}$  is parametrically larger than the global one  $\delta_L = E_{BW}/L \simeq \xi^{1/2}/L$  as soon as  $\xi \ll L$ . For  $\xi \gtrsim L$  there is only one block, therefore  $\delta_\xi = \delta_L$  and all the wave functions are ergodic  $D_2 = 1$ . This happens when  $k > 1/2$  [33]. Therefore in what follows, we focus on the case  $0 \leq k < 1/2$ .

For such  $k$ , the effect of fractal distribution is suppressed due to the strong hybridization in each block and hence the RP all-to-all coupling will hybridize all the energy levels of the blocks in the interval  $\Gamma_1$ , similar to the case of non-fractal disorder  $d = 1$  [17], where  $\Gamma_1$  is the width of the Lorentzian eigenfunction with magnitude,  $\Gamma_1 \sim L^{1-\gamma}$ , which replaces  $\Gamma_d$  in Eq. (7), according to the Fermi's Golden rule. In order to find the wavefunction fractal dimension, we should now compare  $\Gamma_1$  to the block-local  $\delta_\xi$  and global  $\delta_L$ .

For  $\Gamma_1 < \delta_L \ll \delta_\xi$  we have no additional hybridization given by  $\Gamma_1$  and the fractal support set  $L^{D_2}$  is given by  $D_2 = \frac{\ln \xi}{\ln L} = 2k$  similar to a generalized 1D Anderson model [33]. This corresponds to the limit  $\gamma > 2 - k$  and constitutes the fractal IV behavior with Poisson level statistics. For  $\delta_L < \Gamma_1 < \delta_\xi$ , in the energy interval  $\Gamma_1$  there is at most  $O(1)$  levels from each block. Therefore the number of levels, hybridized by  $\Gamma_1$ , will be equal to  $\Gamma_1/\delta_L$ . As a result the fractal support sets  $\sim \xi$  of all  $\Gamma_1/\delta_L$  hybridized wave functions, combined together,

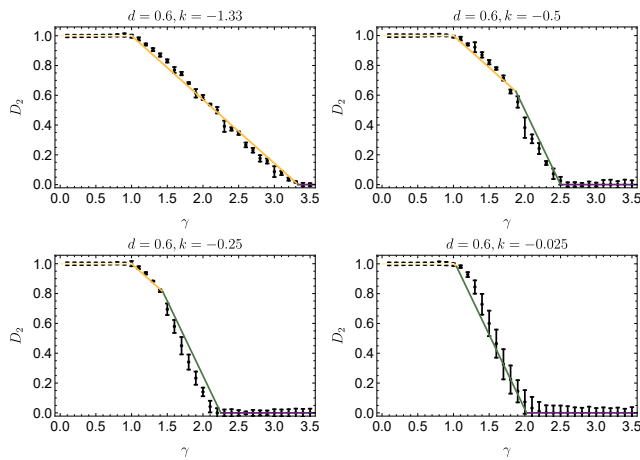


FIG. 3. (a)  $D_2$  vs  $\gamma$  for  $k = -1.33$  which is in Region 3. The solid line is Eq. (6). (b),(c),(d): Three values of  $k$  showing the behavior in Region 2. The solid lines are obtained from Eq. (5), yellow, dark yellow, dark green and purple denote ergodic, fractal I, fractal II and localized phases respectively.

will determine the fractal dimension as (cf. [34])

$$L^{D_2} = \xi \cdot \frac{\Gamma_1}{\delta_L} \Leftrightarrow D_2 = 2 - \gamma + k, \quad (10)$$

where we used the fact that for  $\xi \gg 1$ ,  $\delta_\xi = \xi^{-1/2} \sim L^{-k}$  and that the support set of each eigenstate in each block is  $\xi$ . This behavior constitutes the fractal III RP-like region. For  $\Gamma_1 > \delta_\xi$ , i.e.,  $\gamma < 1 + k$ , the fractal dimension (10) saturates at  $D_2 = 1$  and the wave functions are ergodic. Therefore for  $k > 0$ , we reproduce Eq. (4).

There are several things to note here. Firstly, since  $k > 0$ , in the fractal regime, if present, the fractal dimension of the eigenfunctions are bigger than in the usual RP case [17],  $D_2 > 2 - \gamma$ . Secondly, the ergodic transition now shifts to  $\gamma_{ET}^{(1)} = 1 + k$  and there is no localization transition  $\gamma_{AT}^{(1)}$  for any  $\gamma$ , unlike the standard RP models. What we instead have is a change of level statistics to Poisson statistics at  $\gamma_P = 2 - k$ , while the wave functions are extended with a  $\gamma$ -independent fractal dimension of  $2k$  within each of nearly independent blocks of size  $\xi$  [33, 36]. This is a hallmark of the extensively varying local hopping term. At  $k = 1/2$  the ergodic  $\gamma_{ET}$ , and Poisson  $\gamma_P$ , transitions merge simultaneously with the change of the statistics at  $\gamma > \gamma_P$  from Poisson to Wigner-Dyson and, thus, only ergodic phase survives. These predictions are verified with exact numerics in Fig. 2, where the solid lines represent Eq. (4).

**Regions 2 and 3 ( $k \leq 0 \Rightarrow \kappa \lesssim 1$ ):** In this region, we first need to recompute the localization length  $\xi$  and the hybridized wave functions. This step is crucial, as our primary goal is to accurately compute how hybridization due to the additional term impacts the fractal-distributed disorder  $h_n$ . However, since  $\kappa$  is small, we can employ perturbation theory [35].

If the wave function  $\psi_m(n)$  reaches its maximum at  $n = m$ , then, applying perturbation theory for  $\kappa < 1$ , we obtain  $\psi_m(m \pm 1) = \frac{\kappa}{h_m - h_{m \pm 1}} \psi_m(m) \simeq \psi_m(m) e^{-1/\xi}$ , from which we can extract  $\xi^{-1} = -\ln \kappa + \langle \ln |h_m| \rangle = -\ln(2e\kappa)$  by approximating  $h_n$ s via a box distribution with  $|h_m| < 1/2$  [35]. The corresponding energy shift is given by the second order perturbation theory

$$\epsilon_m = h_m + \sum_{\eta=\pm 1} \frac{\kappa^2}{h_m - h_{m+\eta}}, \quad (11)$$

which typically shifts the diagonal disorder,  $h_m$ , by

$$\exp(\langle \ln |\epsilon_m - h_m| \rangle) \simeq \kappa^2. \quad (12)$$

Beyond the typical shift, the probability to have  $|\epsilon_m - h_m| \sim L^{-b} \ll \kappa^2$ , i.e., with  $b < -2k$ , is given by the probability  $p_b$  to have small  $|h_m - h_{m \pm 1}| \sim L^{b+2k} \ll 1$  [37]. For the regular (uniform or Gaussian) distribution of  $h_m$ ,  $p_b$  is proportional to the small interval,  $|h_m - h_{m \pm 1}|$ , i.e.  $p_b \sim L^{b+2k} \ll 1$ . Thus, among  $L$  differences  $\delta h_n = |h_m - h_{m-1}|$  in the entire sample there are  $M_b \sim L \cdot p_b \sim L^{b+2k+1}$  levels shifted by  $\delta h \equiv |\epsilon_m - h_m| \sim L^{-b}$ . Note that as we have only  $L$  level differences  $\delta h$ , the typical maximal energy hybridization interval  $\delta h_{\max}$ , reaches only at  $M_b \sim L^0$  levels, and scales as  $\delta h_{\max} \sim L^{-2k-1} \ll 1$ . Thus,  $\delta h_{\max}$  will play the role of the crucial energy scale in this regime.

For  $\delta h_{\max} \ll \Gamma_d \ll 1$ , the maximal energy hybridization interval  $\delta h_{\max}$  of the generalized 1D Anderson model is smaller than the one of the fractal RP,  $\Gamma_d$ , given by Eq. (9). Then the RP-hybridization dominates over the effect of nearest-neighbour hopping and the fractal RP results of Ref. 29 are valid. This defines fractal I region and happens at

$$2k + 1 < -\frac{\gamma - 1}{2 - d} < 0 \\ \Leftrightarrow 1 < \gamma < 1 + (2 - d)(2k - 1). \quad (13)$$

and describes the third line in Eq. (5) using  $\Gamma_d$  from (9).

In alignment with this, when  $\delta h_{\max} = \delta_{\text{typ}}$  ( $2k = -1/d - 1$ ), the right-hand side of Eq. (13) equals  $\gamma_{AT} = 2/d$ , and the entire phase diagram resembles that of fractal RP which constitutes Region 3. In Fig. 3(a) we numerically compute the phase diagram of fractal dimension  $D_2$  for  $d = 0.6$  and  $k = 1.33 \sim 2/d$  which shows excellent agreement with our theoretical prediction.

The final case of  $\Gamma_d \ll \delta h_{\max} \ll 1$ , in Region 2, occurs when the hybridization from the 1D hopping affects the fractal diagonal disorder ( $\delta h_{\max} \gg \Gamma_d > \delta_{\text{typ}}$ ,  $-1 - 1/d < 2k < 0$ ), but the corresponding block RP picture is not applicable as the block size  $\xi_\kappa \simeq [\ln(1/(2e\kappa))]^{-1} \ll 1$  is small [35].

The number of fractal levels in the interval  $L^{-b}$  are given by  $L^{1-f(b)}$ , while the number of levels shifted by the same energy  $\delta h \sim L^{-b}$  is  $M_b \sim L^{1+b+2k}$ . This means that



as soon as  $L^{1-f(b)} \ll M_b$ , corresponding to  $b > b_*$ , all the levels in the interval  $L^{-b}$  will be hybridized by at least  $\delta h \sim L^{-b}$  and, thus, losing their fractal distribution they will be redistributed homogeneously on that interval  $L^{-b}$ . Otherwise, if  $L^{1-f(b)} \gg M_b$ , there will just be a measure zero of such hybridization events with a negligible impact on counting.

For small  $b < b_*$  (large enough intervals  $L^{-b}$ ), we have  $L^{1-f(b)} > M_b$ . Since  $f(b) = d \cdot b$  at such  $b < b_*$ , the solution of the equation  $L^{1-f(b_*)} = M_{b_*}$  is given by

$$1 - |2k| + b_* = 1 - d \cdot b_* \implies b_* = \frac{|2k|}{1+d}, \quad (14)$$

which describes the intervals  $L^{-b_*}$ , smaller than which everything in the interval is fully hybridized, i.e.,  $df(b)/db = 1$ . Consequently, the corresponding  $f(b)$ , changed by  $\kappa$ -elements, can be read from the continuity equation at  $b = b_*$  as

$$f(b) = \begin{cases} d \cdot b, & b < b_* \\ b - (1-d)b_*, & b_* < b < b_{**} \end{cases}, \quad (15)$$

where  $b_{**} = 1 + (1-d)b_*$  is determined by  $f(b_{**}) = 1$ .

This means that as soon as the solution of the self-consistency Eq. (8) corresponds to  $f(b < b_*) = d \cdot b$ , i.e., at  $\gamma < \gamma_{FT} = 1 + (2-d)b_*$ , the fractal I solution [29] is still valid. In the opposite case of  $\gamma > \gamma_{FT}$ , substituting  $f(b)$  from Eq. (15) to Eq. (8) gives

$$\Gamma_\kappa = L^{b_{**}-\gamma}, \quad D_2(\gamma > \gamma_{FT}) = 2b_{**} - \gamma \quad (16)$$

It works until the Anderson transition at  $\gamma_{AT}^{(2)} = 2b_{**} = 2 + \frac{2-2d}{1+d}|2k|$ , matches all the other limiting cases and is compiled in Eq. (5). To corroborate the analytical results we plot numerical data for  $D_2$  vs  $\gamma$  for  $k = -0.5, -0.25, -0.025$  in Fig. 3(b)-(d) with the analytical predictions shown in solid lines. Here, dark yellow and dark green solid lines have been used to denote fractal I and II behavior, respectively. The numerical data matches very well with our analytical model.

**Conclusion:** In this letter, utilizing the Rosenzweig-Porter model with fractal disorder, we show that a short-range kinetic term may not always drive the system towards delocalization. In fact, we analytically demonstrate that increasing amplitude of this term results in an unexpected non-monotonic behavior of the localization phase diagram and leads to the re-entrant delocalization. This work elevates the tunability of the fractal phase in RP model, as introduced in [29], to a new level. It shows that by applying local perturbations, a system with fractal diagonal disorder can be driven to localized, fractal, or ergodic states. The underlying mechanism is based on the interplay between the local-in-space tight-binding hopping term  $\kappa$  and the local-in-energy Fermi's golden rule broadening  $\Gamma_d$  in the Rosenzweig-Porter model. In the intermediate regime, these competing delocalization

mechanisms reduce the fractal dimension and can even induce localization. In quantum many-body systems, locality emerges in energy, real, and Hilbert space. Extending this mechanism from random matrix models to such systems could enable competition between localization in different spaces, potentially inducing re-entrant ergodic transitions in many-body setting.

*Acknowledgements:* I. M. K. acknowledges the support by the European Research Council under the European Union's Seventh Framework Program Synergy ERC-2018-SyG HERO-810451. R. G. acknowledges support by EPSRC grant MACON-QC EP/Y004590/1. M. S. acknowledges the support from UK EPSRC award under the Agreement EP/Y005090/1.

\* ucaprgh@ucl.ac.uk

- [1] J. M. Deutsch, Quantum statistical mechanics in a closed system, *Phys. Rev. A* **43**, 2046 (1991).
- [2] M. Srednicki, Chaos and quantum thermalization, *Phys. Rev. E* **50**, 888 (1994).
- [3] D. Basko, I. Aleiner, and B. Altshuler, Metal-insulator transition in a weakly interacting many-electron system with localized single-particle states, *Annals of Physics* **321**, 1126 (2006).
- [4] I. V. Gornyi, A. D. Mirlin, and D. G. Polyakov, Interacting electrons in disordered wires: Anderson localization and low- $t$  transport, *Phys. Rev. Lett.* **95**, 206603 (2005).
- [5] D. A. Abanin, E. Altman, I. Bloch, and M. Serbyn, Colloquium: Many-body localization, thermalization, and entanglement, *Rev. Mod. Phys.* **91**, 021001 (2019).
- [6] D. J. Luitz, N. Laflorencie, and F. Alet, Many-body localization edge in the random-field Heisenberg chain, *Phys. Rev. B* **91**, 081103 (2015).
- [7] D. Sels and A. Polkovnikov, Dynamical obstruction to localization in a disordered spin chain, *Phys. Rev. E* **104**, 054105 (2021).
- [8] J. Šuntajs, J. Bonča, T. c. v. Prosen, and L. Vidmar, Quantum chaos challenges many-body localization, *Phys. Rev. E* **102**, 062144 (2020).
- [9] W. De Roeck, F. Huveneers, M. Müller, and M. Schiulaz, Absence of many-body mobility edges, *Phys. Rev. B* **93**, 014203 (2016).
- [10] J. Z. Imbrie, Multi-Scale Jacobi Method for Anderson Localization, *Communications in Mathematical Physics* **341**, 491 (2016).
- [11] W. D. Roeck, L. Giacomin, F. Huveneers, and O. Prosnjak, *Absence of normal heat conduction in strongly disordered interacting quantum chains* (2024), arXiv:2408.04338 [math-ph].
- [12] P. Sierant, M. Lewenstein, A. Scardicchio, L. Vidmar, and J. Zakrzewski, *Many-body localization in the age of classical computing* (2024), arXiv:2403.07111 [cond-mat.dis-nn].
- [13] V. N. Smelyanskiy, K. Kechedzhi, S. Boixo, S. V. Isakov, H. Neven, and B. Altshuler, Nonergodic delocalized states for efficient population transfer within a narrow band of the energy landscape, *Phys. Rev. X* **10**, 011017 (2020).

- [14] K. Kechedzhi, V. N. Smelyanskiy, J. R. McClean, V. S. Denchev, M. Mohseni, S. V. Isakov, S. Boixo, B. L. Altshuler, and H. Neven, Efficient population transfer via non-ergodic extended states in quantum spin glass, [arXiv:1807.04792](#) (2018).
- [15] P. W. Anderson, Absence of diffusion in certain random lattices, *Phys. Rev.* **109**, 1492 (1958).
- [16] F. Evers and A. D. Mirlin, Anderson transitions, *Rev. Mod. Phys.* **80**, 1355 (2008).
- [17] V. E. Kravtsov, I. M. Khaymovich, E. Cuevas, and M. Amini, A random matrix model with localization and ergodic transitions, *New J. Phys.* **17**, 122002 (2015).
- [18] D. Facchetti, P. Vivo, and G. Biroli, From non-ergodic eigenvectors to local resolvent statistics and back: A random matrix perspective, *Europhys. Lett.* **115**, 47003 (2016).
- [19] K. Truong and A. Ossipov, Eigenvectors under a generic perturbation: Non-perturbative results from the random matrix approach, *Europhys. Lett.* **116**, 37002 (2016).
- [20] C. Monthus, Statistical properties of the Green function in finite size for Anderson localization models with multifractal eigenvectors, *J. Phys. A: Math. Theor.* **50**, 295101 (2017).
- [21] E. Bogomolny and M. Sieber, Eigenfunction distribution for the Rosenzweig-Porter model, *Phys. Rev. E* **98**, 032139 (2018).
- [22] P. von Soosten and S. Warzel, Non-ergodic delocalization in the Rosenzweig-Porter model, *Letters in Mathematical Physics*, **1** (2018).
- [23] D. Venturelli, L. F. Cugliandolo, G. Schehr, and M. Tarzia, Replica approach to the generalized Rosenzweig-Porter model, *SciPost Phys.* **14**, 110 (2023).
- [24] M. Hopjan and L. Vidmar, Scale-invariant critical dynamics at eigenstate transitions, *Phys. Rev. Res.* **5**, 043301 (2023).
- [25] G. De Tomasi, I. M. Khaymovich, F. Pollmann, and S. Warzel, Rare thermal bubbles at the many-body localization transition from the Fock space point of view, *Phys. Rev. B* **104**, 024202 (2021).
- [26] M. Tarzia, Many-body localization transition in Hilbert space, *Phys. Rev. B* **102**, 014208 (2020).
- [27] M. Hopjan and L. Vidmar, Scale-invariant survival probability at eigenstate transitions, *Phys. Rev. Lett.* **131**, 060404 (2023).
- [28] B. Altshuler and V. Kravtsov, Random Cantor sets and mini-bands in local spectrum of quantum systems, *Annals of Physics*, 169300 (2023), in press.
- [29] M. Sarkar, R. Ghosh, and I. M. Khaymovich, Tuning the phase diagram of a rosenzweig-porter model with fractal disorder, *Phys. Rev. B* **108**, L060203 (2023).
- [30] N. Rosenzweig and C. E. Porter, "Repulsion of energy levels" in complex atomic spectra, *Phys. Rev. B* **120**, 1698 (1960).
- [31] See Supplemental Material at [URL will be inserted by publisher] for technical details, which includes Refs. [].
- [32] G. De Tomasi and I. M. Khaymovich, Non-Hermitian Rosenzweig-Porter random-matrix ensemble: Obstruction to the fractal phase, *Phys. Rev. B* **106**, 094204 (2022).
- [33] A. K. Das, A. Ghosh, and I. M. Khaymovich, Absence of mobility edge in short-range uncorrelated disordered model: Coexistence of localized and extended states, *Phys. Rev. Lett.* **131**, 166401 (2023).
- [34] R. Barney, M. Winer, C. L. Baldwin, B. Swingle, and V. Galitski, Spectral statistics of a minimal quantum glass model, *SciPost Phys.* **15**, 084 (2023).
- [35] F. Izrailev, S. Ruffo, and L. Tessieri, Classical representation of the one-dimensional Anderson model, *Journal of physics A: Mathematical and general* **31**, 5263 (1998).
- [36] W. Tang and I. M. Khaymovich, Non-ergodic delocalized phase with Poisson level statistics, *Quantum* **6**, 733 (2022).
- [37] Note that  $b > -2k > 0$  is not achievable, because  $|h_m - h_{m\pm 1}| \leq O(1)$ .

## Appendix A: Details of Fractal RP model

Let us provide a brief description of the fractal RP model. In this special RP model, we consider the diagonal elements ( $h_n$ ) to be chosen from certain (multi)fractal distribution (e.g., on a Cantor set [28, 29]). In such a case, one can just count how many  $n$ s are distributed in the interval  $|E - h_n| \in [L^{-b-db}, L^{-b}]$ , parameterized by  $b \geq 0$ ,

$$L^{1-f(b)} \equiv \# \{n : |E - h_n| \in [L^{-b-db}, L^{-b}]\} \quad , \quad (\text{A1})$$

with a certain  $f(b)$ , characterizing the above multifractal. We assume that the overall bandwidth of the diagonal elements is  $O(1) = O(L^0)$ , thus, in general  $f(0) = 0$ .

For example, if we choose  $h_n$ s from a Cantor set,

$$f(b) = d \cdot b \quad , \quad (\text{A2})$$

with  $d$  being a Hausdorff dimension of the Cantor set. The usual uncorrelated random case [17] corresponds to  $d = 1$ , while the non-Hermitian complex one [32] gives  $d = 2$ . In principle, one can consider any values of  $d$  in the interval  $0 \leq d \leq 2$  if one considers the non-Hermitian matrices with complex entries [32].

In general,  $f(b)$  has the following properties

- $f(0) = 0$  and  $df(b)/db \geq 0$  as we assume that all  $L$  diagonal elements are within the bandwidth  $L^0$  and their number decays with the decaying interval  $|E - \epsilon_n| \sim L^{-b}$ ;
- $f(\Delta_{typ}) = 1$  with  $\delta_{typ} \sim L^{-\Delta_{typ}}$  being the typical level spacing of the set. Note that in the real case the mean level spacing is given by  $\delta \sim L^{-\Delta}$ , with  $\Delta = 1$ , while in the complex case  $\Delta = 1/2$ .
- Following the previous examples, at any  $b$  the derivative  $df(b)/db$  cannot be larger than 1 for the real case and 2 for the complex one.

## Appendix B: Phase diagram for other values of $d$

In Fig. 4 we show a comparison between how the reentrant phase diagram varies upon variation of the dimension of the fractal diagonal disorder  $d$ . In Fig. 4 we plot

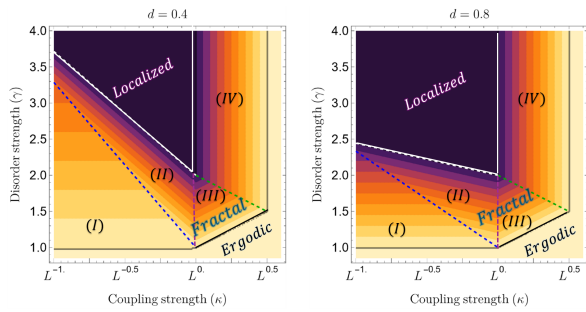


FIG. 4. Plots showing variation of  $D_2$  vs disorder strength represented by  $\gamma$  and nearest-neighbor coupling strength  $\kappa$  for fractal disorder with fractal dimensions left:  $d = 0.4$  and right:  $d = 0.8$ .

the scenario for (a) a low,  $d = 0.4$ , and (b) high,  $d = 0.8$ , fractal dimension of the on-site disorder. Note that  $d > 1$  gives same results as  $d = 1$ . We immediately notice that as the  $d$  increases the localized phase increases and the re-entrant region shrinks on the phase diagram. This is completely consistent with expectations as to put it briefly, the reentrance happens due to the sensitivity of the local-in-energy Fermi's golden rule broadening  $\Gamma_d$  to the fractal on-site disorder and the interplay of the former  $\Gamma_d$  to the local-in-space hopping term  $\kappa$ , fully insensitive to any fine spectral structure. However since  $d = 1$  has the same characteristic behavior as the standard RP model, no additional fine spectral structure emerges at  $d = 1$ . Thus, it should come as no surprise that the region shrinks as increase  $d$  towards that value.